PILOT: a balloon-borne experiment to measure the polarized FIR emission of dust grains in the interstellar medium

R. Misawa[a] and J-Ph. Bernard[a] and P. Ade[e] and Y. André[g] and P. deBernardis[d] and M. Bouzit[b] and M. Charra[b] and B. Crane[b] and J.P. Dubois[b] and C. Engel[a] and M. Griffin[e] and P. Hargrave[e] and B. Leriche[b] and Y. Longval[b] and S. Maes[a] and C. Marty[a] and W. Marty[a] and S. Masi[d] and B. Mot[a] and J. Narbonne[a] and F. Pajot[b] and G. Pisano[e] and N. Ponthieu[f] and I. Ristorcelli[a] and L. Rodriguez[c] and G. Roudil[a] and M. Salatino[d] and G. Savini[e] and C. Tucker[e]

[a]Institut de Recherche en Astrophysique et Planetologie (IRAP), 9 Av du Colonel Roche, BP 4346, 31028 Toulouse cedex 4;
[b] Institut d'Astrophysique Spatiale (IAS), Bât 121, Université Paris XI, Orsay, France;
[c]CEA/Saclay, 91191 Gif-sur-Yvette Cedex, France;
[d]Universita degli studi di Roma "La Spienza", Dipartimento di Fisica, P.le A. Moro, 2, 00185, Roma, Italia;
[e]Department of Physics and Astrophysics, PO BOX 913, Cardiff University, 5 the Parade, Cardiff, UK;
[f]Grenoble University, Grenoble, France;
[g]Centre National des Etudes Spatiales, DCT/BL/NB, 18 Av. E. Belin, 31401 Toulouse, France;

ABSTRACT

Future cosmology space missions will concentrate on measuring the polarization of the Cosmic Microwave Background, which potentially carries invaluable information about the earliest phases of the evolution of our universe. Such ambitious projects will ultimately be limited by the sensitivity of the instrument and by the accuracy at which polarized foreground emission from our own Galaxy can be subtracted out. We present the PILOT balloon project which will aim at characterizing one of these foreground sources, the polarization of the dust continuum emission in the diffuse interstellar medium. The PILOT experiment will also constitute a test-bed for using multiplexed bolometer arrays for polarization measurements. We present the results of ground tests obtained just before the first flight of the instrument.

Keywords: PILOT, balloon-borne, polarization, submilimeter, instruments

1. INTRODUCTION

Current theories predict that, much before recombination, well within the first second after the Big-Bang, the universe underwent a period of extremely fast expansion called inflation. During this phase, the size of the universe grew from microscopic to macroscopic almost instantly. The inflation theory provides a natural explanation to several paradoxes of the big-bang theory, and is therefore favoured by many cosmologists and particle physicists. Observations of the intensity of the CMB anisotropies cannot reveal the inflation phase, since all information from periods prior to the last scattering surface was lost. If they were not so difficult to detect by nature, density waves generated during the inflation would bring us invaluable information about these very early phases. Luckily, the interaction between the quadrupole anisotropies induced by primordial gravitational waves and the CMB photons at the last scattering surface is expected to have polarized a tiny fraction of the CMB light (called B-modes). Measuring this polarized signal would allow cosmologists to look behind the curtain of the last scattering surface and would alleviate degeneracies in the present cosmological parameter determination.

Further author information: (Send correspondence to J.P.B.)
J.P.B.: E-mail: Jean-Philippe.Bernard@irap.omp.eu, Telephone: 33 (0)5 61 55 75 38
R.M.: E-mail: rmisawa@irap.omp.eu, Telephone: 33 (0)5 61 55 75 38

However, the CMB B-modes are extremely weak. Depending upon the energy scale at which inflation actually occurred, they may not even be observable in the foreseeable future. In any case, their detection promises to be the next major challenge of observational cosmology and the next major step forward for cosmology and fundamental physics.

Several mission concepts for future satellite missions to measure B-modes are already under study in the USA and Europe (such as EPIC, Einstein Probe for Inflationary Cosmology or CMBpol). The main limitations to CMB polarization measurements will be the sensitivity of the measurements and the confusion with unrelated foreground polarized emission. The current observation sensitivity in the microwave domain is already limited by photon noise from the CMB radiation itself, so that it can only be improved by massively increasing the number of detectors. This will require using multiplexed bolometer filled arrays of very large format. Such devices are slowly becoming available. Note however that systematic effects induced by the instrument itself will also have to be controlled down to very low levels in order to achieve ultimate sensitivities. Confusion arises from polarized emission produced by several other astronomical sources. First, the quadrupole anisotropies caused by the electron motion near density perturbations at the time of decoupling (so called scalar perturbations) is expected to produce additional CMB polarization, which is not directly linked to density waves and inflation. Unlike for B-modes, the associated polarized signal (called E and TE-modes) is expected to be correlated with the density, and therefore with the CMB intensity fluctuations. Also, they are expected to have a different parity than that of the B-modes, which could allow separation of the various components, despite the fact that B-modes are much weaker than the E and TE-modes. A second source of foreground is the polarized emission originating within our own Galaxy, either from sub-micron size dust particles (polarized dust emission) or gas particles (synchrotron radiation) interacting with the magnetic field of our Galaxy. The 3-year WMAP results[1] have shown that, already for E and TE modes, correcting for the contribution of polarized foreground emission is a crucial step towards an accurate measurement of CMB polarization. At the accuracy levels required to detect B-modes, no piece of sky will be clean, even at high galactic latitude, and polarized foregrounds will have to be precisely understood and removed before any cosmological interpretation of the data can take place. Although a very accurate knowledge and understanding of polarized foreground signals will be needed, their amplitude and characteristics are presently very poorly constrained by observations.

Many experiments are currently engaged in the measurement of polarized CMB and the search for B-modes, either from the ground (e.g. QUaD, BICEP, Clover, BRAIN, QUIET, ...) or from balloons (e.g. Bar-Sport, EBEX, Spider, ...). However, none of them is actually designed specifically to address the foreground contamination issue. Here, we present the PILOT experiment, which will tackle the problem of precisely measuring the polarized emission from dust grains in the diffuse InterStellar Medium (ISM).

2. DUST POLARIZATION

The ISM is populated by very tenuous gas (essentially neutral Hydrogen, but also more complex molecules) and dust grains of sub-micron size which are composed of solid, amorphous silicates and graphite. These grains absorb starlight mainly in the UV and visible, are heated to 15-30 K in the diffuse ISM and radiate continuum emission in the Far-Infrared to Sub-millimeter wavelength range, where they dominate the total sky emission. Dust particles are believed to have somewhat elongated shapes. In the presence of the faint magnetic field (a few micro-gauss) that pervades in the ISM, several processes contribute to make dust grains rotate about their minor axis, which then partially aligns with respect to the magnetic field lines. This partial alignment of dust grains causes preferential absorption of starlight along the major axis of the grains, so that unabsorbed star light appears slightly polarized along the field direction. Similarly, emission by partially aligned dust grains causes a fraction of the thermal emission to be linearly polarized in a direction orthogonal to the magnetic field line, as projected on the sky.

For a long time, dust emission polarization measurements remained very scarce and suffered from large biases. Ground-based observations in the visible allowed to measure the polarization in absorption toward stars,[2] but were restricted to selected directions on the sky where bright stars are present. Due to their low sensitivity, polarization measurements in emission obtained from large telescopes on the ground allowed to probe only the brightest regions of the sky, in the immediate vicinity of star forming regions. These regions show features which are specific to extreme environments where stars form, and which are not representative of the physical effect

which will dominate in more diffuse regions. In particular, it is possible that the increased gas density in those regions somewhat disrupts the grain alignment with the magnetic field, which could explain the saturation of the polarization fraction observed with rising column density in those regions and the very low polarization fractions (of the order of 2%) observed there.[3]

The balloon experiment ARCHEOPS [4] measured the dust emission polarization at 353 GHz over a large fraction of the milky way.[5] A significant polarized signal was detected toward several individual regions of the Galactic plane, where the intensity is high enough for its polarization to be measured. They correspond to individual Molecular Clouds (MCs). The polarization degree towards those regions is larger than 5%, stronger than previously expected, and is sometimes larger than any region of the sky already measured (consistent with polarization degrees up to 10%). Note that these figures are average values taken over fairly large regions of the sky, of the order of 3-50 square degrees. Note also that currently available techniques from the ground do not presently allow the detection of polarization over such large areas with moderate to low intensity. In principle, they may correspond to regions where the geometry of the magnetic field orientation is very coherent and close to the plane of the sky over large volume areas. They could also correspond to molecular clouds where the dust properties vary and grain alignment is favored. Despite its success, the ARCHEOPS limited sensitivity did not allow a direct determination of the polarization towards diffuse regions at higher galactic latitude.

Recently, the Planck satellite measurements have finally revealed the structure of dust polarization over large regions of the sky. A tight correlations between polarization in VIS extinction towards selected stars and the corresponding submm emission ([6]) confirms that the same grains are producing both. The large ratio of submm to VIS polarization challenges current dust models. Several regions were identified with polarization fractions at 353 GHz up to almost 20% ([7]). These highly polarized regions may correspond to regions where the geometry of the magnetic field orientation is very coherent and close to the plane of the sky over large volume areas. Their existence confirms that dust in diffuse regions can be efficiently aligned and intrinsically polarized to much higher fractions than previously expected. The Planck data also revealed that the direction of the apparent dust emission polarization, which traces the sky projection of the magnetic field averaged over the LOS, is generally homogeneous in large polarization fraction regions, and rotates abruptly in low polarization fraction regions. The high rotation regions draw spectacular filamentary features. These results indicate that the 3D geometry of the magnetic field along the LOS is a key parameter determining the apparent dust polarization fraction. This was confirmed by a comparison with predictions from MHD simulations that reproduces the observations ([8]). Inspection of the spectral dependence of the polarization fraction over the Planck spectral range ([6]) indicates a weak but steady decline of the polarization fraction with frequency that could reflect either dust properties, such as metallicinclusions in dust grains, or progressive reduction by unproperly understood additional emission sources, such as spinning dust or free-free emission. Finally, the expected correlation between dust and synchrotron polarized emission, although present, is rather poor ([7]), suggesting that dust and high energy cosmic rays generally sample quite different regions of the LOS and magnetic field directions.

3. PILOT DESCRIPTION

PILOT (Polarized Instrument for the Long-wavelength Observations of the Tenuous ISM: http://pilot.irap.omp.eu , is a project of a balloon-borne astronomy experiment to study the polarization of dust emission in the diffuse ISM in our Galaxy.

The PILOT instrument will allow observations in two photometric channels at wavelengths 240 μm (1.2 THz) and 550 μm (545 GHz) at an angular resolution of a few arcminutes. We will make use of large format bolometer arrays, newly developed for the PACS instrument on board the Herschel satellite. With 1024 detectors per photometric channels and photometric bands optimized for the measurement of dust emission, PILOT is likely to become the most sensitive experiment for this type of measurements. The proposed method to measure polarization using filled arrays has been validated by end-to-end simulations. The PILOT experiment will take advantage of the large gain in sensitivity allowed by the use of large format, filled bolometer arrays at frequencies more favorable to the detection of dust emission. Its sensitivity will surpass that of ARCHEOPS and even that of Planck (by a factor about 20-30) for a given column density of interstellar matter. It will prefigure that of future cosmology experiments. Note that PILOT will be the only instrument able to measure the polarization

properties of dust emission in the FIR, since none of the Herschel satellite instrument will be sensitive to polarization.

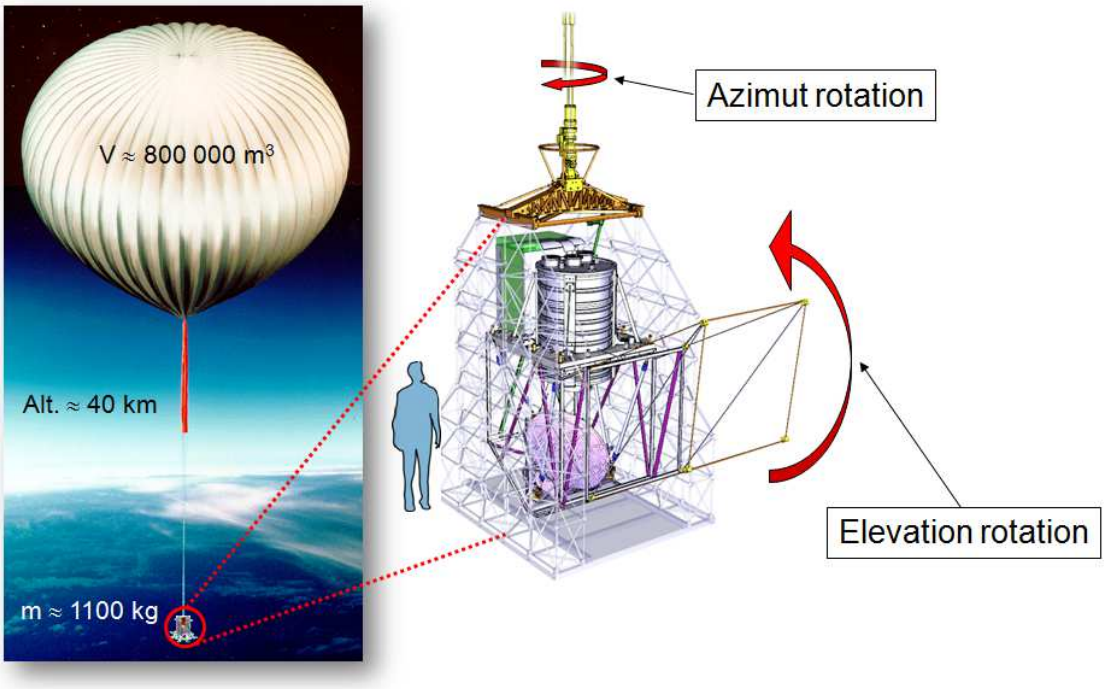

Figure 1. Schematic view of the PILOT gondola. The cryostat (cylinder on top) and the primary mirror are attached to the pointed load, which can rotate around its elevation axis in order to change the elevation of the submm optical axis. Motion around the flight chain will be ensured by the azimuth swivel. Optical baffles and thermal protection screens surrounding the experiment are not shown.

3.1 Science Goal

The observations of PILOT have two major scientific objectives. On the one hand, they will allow us to constrain the large scale geometry of the magnetic field in our Galaxy and to study in details the alignment properties of dust grains with respect to the magnetic field. In this domain, the measurements of PILOT will be complementary with those of Planck at longer wavelengths. In particular, they will bring information at a higher angular resolution, which is critical in crowded regions such as the Galactic plane. They will allow us to better understand how the magnetic field is shaping the ISM material on large scale in molecular clouds, and the role it plays in the gravitational collapse leading to star formation. On the other hand, the PILOT observations will allow us to measure for the first time the polarized dust emission towards the most diffuse regions of the sky, where the measurements are the most easily interpreted in terms of the physics of the dust. In this particular domain, PILOT will play a role for future CMB missions similar to that played by the Archeops experiment for Planck. The results of PILOT will allow us to gain knowledge about the magnetic properties of dust grains and to the structure of the magnetic field in the diffuse ISM that will be necessary to a precise foreground subtraction in future CMB measurements. For instance, one of the major objectives is to test if the dust polarization degree changes with wavelength, as some ground observations towards dense regions seem to indicate (see[9]). Dust models which invoke the existence of two separate dust components at different temperatures in the ISM to explain the sub-mm emission of our Galaxy (e.g.[10]) are likely to produce such changes, since different types of grains dominate the FIR and submm emission. However, most recent models advocating for the submm emission being produced by low energy transitions in the amorphous material composing the grains ([11]) are expected to produce very little variations of the polarization properties with wavelength, since the same dust grains dominate the emission over the whole spectrum. The PILOT measurements, combined with those of Planck at longer

wavelengths, will therefore allow us to further constrain the dust models. The outcome of such studies will likely impact the instrumental and technical choices for the future space missions dedicated to CMB polarization.

PILOT will not only detect polarized dust emission, but will also measure its total intensity with high accuracy. When combined with the IRAS and AKARI all-sky surveys at 100 μm and 160 μm respectively, the large scale survey performed with the PILOT experiment at 240 μm will be important in deriving the dust temperature, which is a critical quantity for all dust studies. In combination with the PLANCK data at longer wavelengths,[12–14] and the PILOT data at 500 μm, this will be used to study the dust emissivity slope over large areas of the sky. Note that accurate determinations of the dust temperature distribution are obviously be possible with the Herschel satellite data, but have to be focused on limited sky areas, since the largest surveys with Herschel cover a small fraction of the sky, with the Herschel galactic plane survey (HiGal) covering only 2 degrees in galactic latitudes.[15] Scientific by-products of the PILOT experiment will also include a large point-source catalog (several hundred sources should be detected per hour).

3.2 Instrument description

PILOT is a balloon-borne experiment being designed to fly at a ceiling altitude of around 40 km (4 hPa pressure) in the stratosphere. The experiment will be carried by a generic CNES stabilized gondola with altazimuthal coarse pointing control, as shown in Fig. 1. Mapping of the sky will be accomplished by rotating the gondola over a large azimuth range ($\pm 30^o$) at constant elevation, in order to reduce the residual atmospheric contribution. The elevation of the pointed payload can range from 20^o to 60^o. The fine attitude of the instrument and the effective pointing directions will be constructed a posteriori, using the signal from a fast, large format CCD stellar sensor co-aligned with the sub-mm axis. The fastest (1.2^o/s) rotation speed for the azimuth scanning is a compromise between, on the one hand, the need to cover a large amplitude and to reduce the instrument drifts, and, on the other hand, the need to distinguish point sources detection from parasitic "spikes", and respect both the detectors and the stellar sensor response times. The total gondola weight will be of the order of 1100 kg.

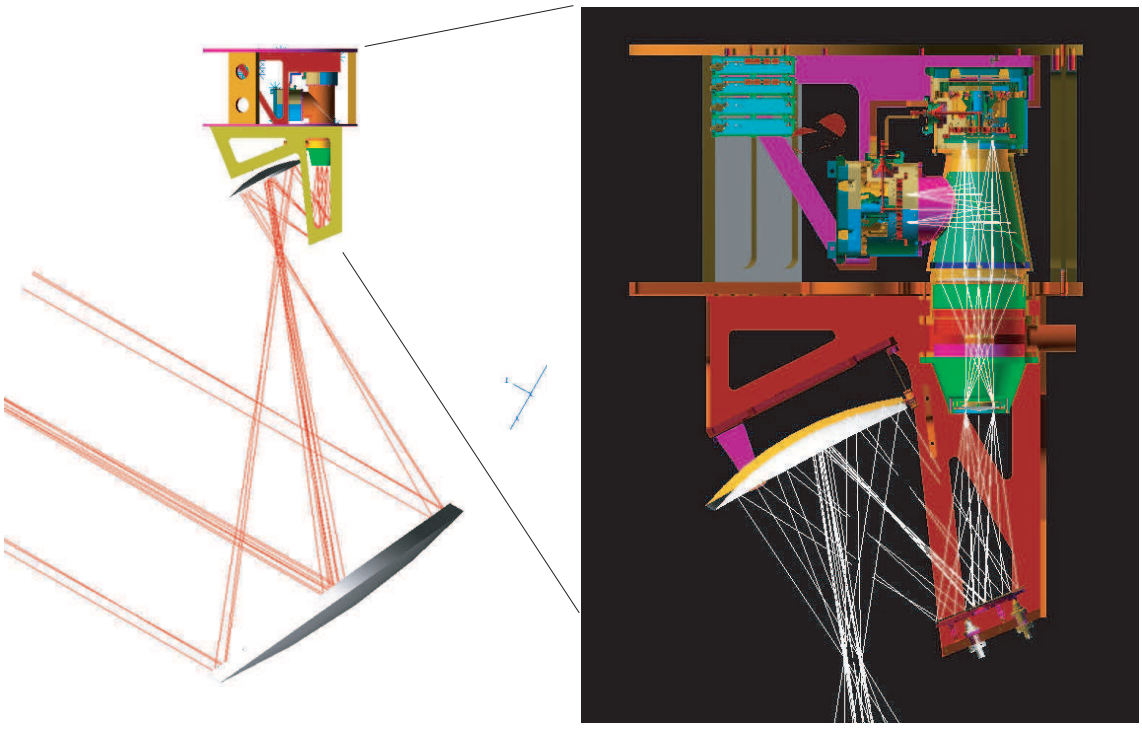

Figure 2. Schematic view of the PILOT Optics and Photometer. Left: Full view showing the off-axis primary mirror (bottom) and the cryostat (top). The incoming beam is focalized by the primary on the entrance window of the cryostat. Right: blow-up view of the cold optics inside the cryostat. The two orthogonal polarization components are split by a tilted polarizer towards the transmission (top) and reflection (left) bolometer array housings.

The optics of PILOT is designed to provide an instantaneous field of view of $1^o \times 0.76^o$, with an equivalent focal distance of 1790 mm and a F/2.6 numerical aperture. The angular resolution of the instrument ($< 3.5'$) has been chosen as a compromise between the need of having a resolution similar or better than that of the IRAS satellite and the aim of surveying large portions of the sky per flight, with a telescope size limited by weight constraints. The optics consists of an off-axis Gregorian telescope with a diameter of $\simeq 800$ mm and a reimaging refractive objective (see Fig. 2). The telescope is composed of an off-axis paraboloid primary mirror and a off-axis ellipsoid secondary mirror, both made out of Aluminium. The combination is equivalent to an on-axis parabolic system (Mizuguchi-Dragone condition) in order to minimize depolarization effects. The reimaging refractive objective consist of two lenses acting as a telecentric objective, reimaging the focus of the telescope onto the detectors. A Lyot-Stop is located between the lenses at a pupil plane which is conjugated to the primary mirror. The polarization will be measured using a rotating half-wave plate located next to the Lyot-stop and a fixed polarizer in front of the detectors. The fixed polarizer will be tilted to about 45^o in order to reflect one polarization component on one bolometer housing (reflection array) and to transmit the other polarization component on a second bolometer housing (transmission array). This optical configuration is optimized to have good optical performances and to minimize straylight, both internal and external to the cryostat.

In order to reduce the background level on the bolometers, all optical elements except the primary mirror will be located inside a large liquid He cryostat, cooled down to 2 K using a pumped He bath. The detectors will be further cooled down to 0.3 K using an He^3 closed cycle fridge mounted on the 2 K plate. The cryostat will also allow the thermalization on the different cryogenic stages of more than 150 wires necessary to carry the scientific and house-keeping signals on their way out toward the warm electronics. Optical filters will be mounted both next to the entrance window of the cryostat and close to each detector housing, where the bandpass selection of each photometric channel will be performed, so that half of each (reflection and transmission) detector housing operates in one of the two photometric channels (240 and 550 μm).

We will use the filled bolometer arrays which have been developed by CEA/LETI for the PACS instrument on board the Herschel satellite (see Fig. 3). These incorporate fully multiplexed readout at 300 mK. They are produced as filled arrays of 16*18 detectors. They are then assembled into a mechanical housing which ensures cooling at 300 mK and includes the multiplexing and amplification circuits. We will use one such housing per polarization component, each channel being equipped with 4 matrices or 1024 individual detectors. The Noise Equivalent Power (NEP) of each bolometer is of the order of a few $10^{-16}\, W/\sqrt{Hz}$, including noise from the readout electronics. The readout speed of this type of array is however much slower than for individual bolometers such as those which equip the ARCHEOPS and Planck experiments.

Since the polarization measurements are derived from differences between bolometer signals, either instantaneous of different detectors, or of the same detector at different instants, very accurate intercalibration of the bolometer signal at all timescales is mandatory. This will be achieved though the use of an Internal Calibration Source (ICS). We will use the spare model of the SPIRE internal calibration source developed for the SPIRE instrument on board Herschel. This source, passed through a hole of the flat mirror within the cryostat, will shine light through the lenses (see Fig. 3) so as to fully illuminate both arrays with a highly reproducible illumination pattern. It will be used between sky scans to calibrate the variations of the response flat-field of the detectors.

3.3 Polarization measurement and intercalibrations

The polarization will be measured using a combination of a rotating half-wave plate and the fixed analyzer grid positioned in front of the detector housings. This is a classical design in which the polarized part of the incident light is phase-shifted by the wave-plate and selectively transmitted by the analyzer. It produces a modulation of the polarized signal at twice the rotation frequency of the plate. Such systems are often used at rotation frequencies of a few Hertz followed by in-phase analysis of the bolometer signal. However, such a use has one main disadvantage: Given that the instrumental background can easily be 10^5 times higher than the polarized signal to be measured, any fluctuation of the background introduced by the rotating plate, such as anisotropies of the plate transmission, can easily produce a signal in excess of the astrophysical polarized signal and be mistaken for polarized signal. For mapping experiments where scanning of the sky is obtained by constant drifting, the polarization modulation ends up being at a frequency close to that corresponding to the sky structures to be measured. If well adapted to fast readout single bolometers, this technique is not necessarily the most optimal

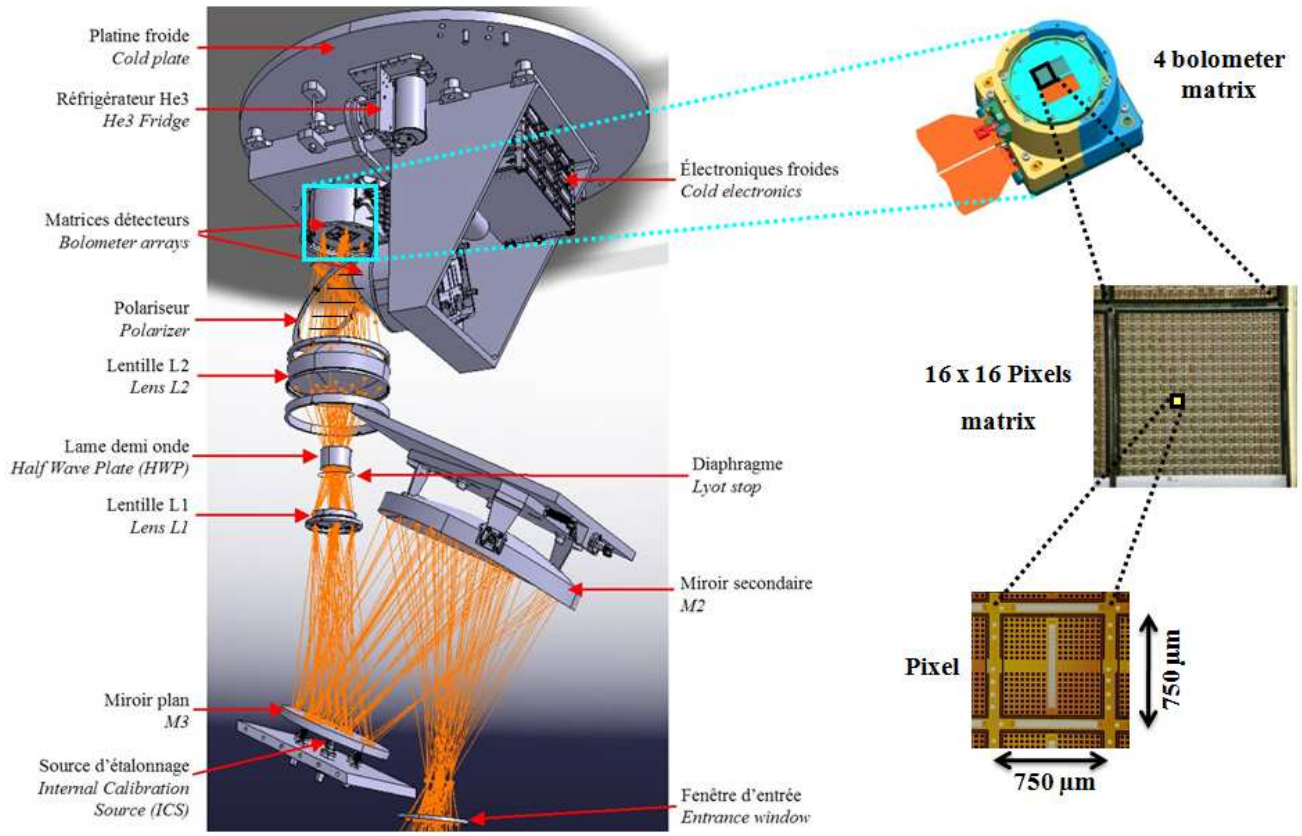

Figure 3. Schematic view of the cryostat showing the location of the cold optical elements, Internal Calibration Source (ICS) and bolometer mechanical housing for both photometric channels. The inner structure of one of the bolometer housing is shown. The closeup view reveals the structure of several bolometers of the array.

for slower bolometer arrays. For PILOT , we plan to use a stepping wave-plate, the angular position of which (at least 2 are necessary to measure polarization) will be changed at the end of each scan on the sky. This measurement method is similar to what is achieved using Polarization Sensitive Bolometers (PSBs) or Orto-Mode Transducers (OMT) pairs. The I and Q Stokes parameters are measured at a given time t, through a differential measurement and I and U parameters are then measured at a later time t', the main difference being that, in our case, the time difference between the two measurements is the time separation between successive scans. This is equivalent to modulating the polarized signal at a very low frequency, which is well below those associated to the structures to be detected in the maps. We therefore expect that the background signal should be slightly different between the different positions of the plate, but this will contribute a constant offset between individual scans, which can be removed during data processing and will not affect the structures observed along the scan. A second advantage is that, individual scans being obtained at a constant direction of the analyzer, redundancy in the scans can be used to intercalibrate the response of individual bolometers (response flat-field) at any time. This will be used to monitor the possible variations of the response flat-field between successive calibration sequences on the ICS. However, such low frequency modulation does not necessarily freeze the low frequency drifts of the bolometer noise (so called 1/f noise) or fluctuations of the residual atmospheric signal with sufficient accuracy. Results of numerical simulations for these contributions indicate that this will not affect our ability to recover the polarization intensity, partly because the 1/f noise of the bolometers used is low.

4. GROUND TESTS

The aim of the PILOT ground tests was to validate the instrument behavior and to optimize its performances. These tests were realized in a clean room at the CNES facilities in Toulouse, France. They are described in the next subsections. Since the background falling on the detectors is much stronger in the ground configuration

than at ceiling altitude, and the detectors are optimised for a moderate background, of the order of 5 pW/pix, we inserted an additional filter in the filter stack, which attenuates a large fraction of the radiation by a factor of 20. The spectral transmission of the attenuator was measured with the FTS and set according to the predictions of a photometric model of the instrument taking into account external and internal sources of emission, as well as the transmission of the various optical filters, as measured at the subsystem level.

For these tests, the PILOT pointed load was aligned with the IRAP submillimeter bench (see the experimental setup in Fig. 4). The optical bench is composed of a high intensity lamp (Mercury plasma lamp) at the focus of a $\phi = 1\,\mathrm{m}$ diameter Newton telescope with a focal length of 5340 mm, delivering a $1m$ diameter collimated beam, and acting as a point source at infinite distance. The source is modulated by a rotating chopper. The source is mounted on a motorized 2D moving plate and can be moved at the focus of the system, so that it can be displaced over a limited range without moving the telescope.

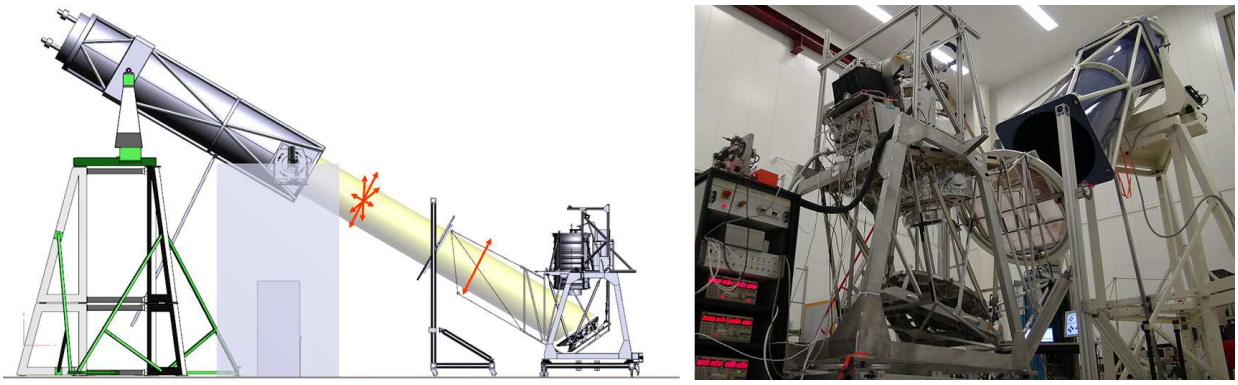

Figure 4. Optical bench used to characterize polarization properties of the instrument, showing from left to right, the IRAP $\phi = 1\,\mathrm{m}$ collimator, the large format ARCHEOPS polarizer and the PILOT pointed load. The polarizer can be removed for intensity only measurements.

4.1 OPTICAL PERFORMANCES

4.1.1 FOCUS

The requirement on the overall optical quality of the PILOT instrument is that the alignment between the primary mirror and the photometer requires accuracy of the order of $\pm 300\mu m$ for the focus, and a maximum mismatch of 0.06° between optical axes of their optical axes. The requirement must be satisfied at all time during the observations at ceiling altitude, while the elevation of the pointed load is changed and the temperature of the structure evolves. This is actually one of the most stringent requirements for the experiment.

Fulfilling this requirement has implied a series of actions: First, precise characterization of the mechanical and optical properties of the primary mirror alone and of the photometer alone have been carried. The mirror characterization[16] was performed with the submillimeter test bench shown in Fig. 4 with no polarizer. The photometer optical characteristics were determined using a ZEMAX simulation and $3D$ measurements. Second, specific means and an efficient procedure to align the two subsystems, both in the laboratory and at the launch site, are needed. To perform this alignment, the primary mirror is mounted on an hexapod, which allow six degrees of freedom for the adjustment while maintaining the stiffness of the system. A numerical model of this mechanism allows a fast convergence of the optical alignment. The relative position of the two subsystems is checked by measuring, using a laser tracker system, of a series of optical reference balls associated with the mirror and the photometer. Third, despite the fact that the whole structure connecting the photometer and M1, and M1 itself are made of the same material (aluminium), which limits differential dilatation, the optical system is off-axis and no perfect compensation is possible. In order to control the optical alignment during the flight, a thermal model of the instrument has been developed. Before the launch, the use of this model knowing the flight conditions, will allow to correct for the expected displacement, compensating to first order the effect of the thermal expansion of the mechanical structure expected at ceiling altitude. Fourth, deformation of the holding structure due to gravity at the various elevations of the pointed load has been modelled (using a finite elements

analysis based on Nastram). The deformations are expected to be somewhat lower than thermal deformations. They have also been measured during tests.

In order to determine the best optical alignment of M1 with respect to the photometer, we have performed a series of defocusing along three orthogonal axes, around the best theoretical focus supplied by the Zemax model. The Z defocusing direction corresponds to the optical axis of the photometer while X and Y are orthogonal to it. To estimate the impact of defocusing on the optical performance, several parts of the focal plane have been explored with the collimator for each defocus. The source PSF was fitted in the obtained images, in order to measure the changes in the Full Width Half Maximum (FWHM) and encircled energy as a function of defocusing distance. The best focus position was determined as the position of minimum PSF FWHM.

Figure 5 shows an example of the FWHM of the observed source on an array at some defocus positions, the defocus distance measured from the initial position.

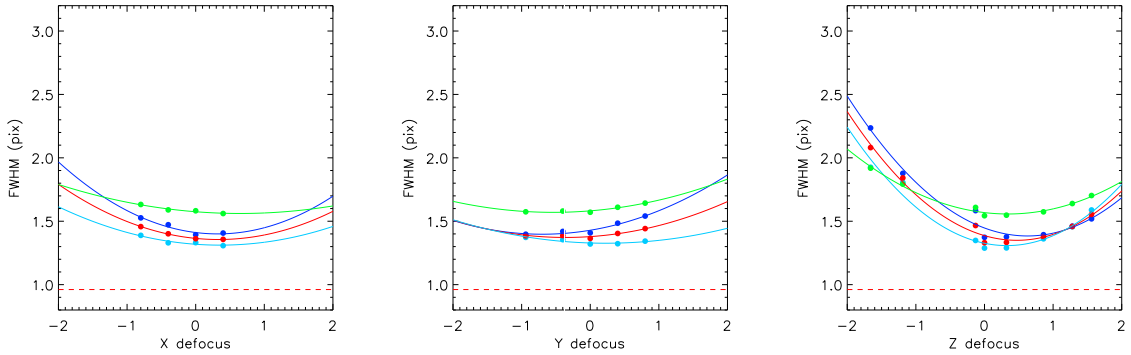

Figure 5. Measured FWHM of the collimator source, as a function of the defocus distance along the X (right), Y (center) and Z (left) on PILOT array #2. FWHM values are in array pixel units. The horizontal dashed lines show the diffraction limit. Blue lines show the FWHM along the X axis and Cyan lines show the FWHM along the X axis, the red lines show averaged FWHM of X and Y axis and green lines show the FWHM values derived from a circular profile of the PSF.

4.1.2 POINT SPREAD FUNCTION

The collimator is used to simulate a point source at infinite distance which sky position is accurately known through laser tracker measurements. An example of the observed PILOT Point Spread Functions (PSF) is represented in Fig. 6 for a transmission and a reflection array. The origin of the position offset is the peak intensity position of the PSFs along the x and y axis. The PSFs are axial symmetries and along the x axe and the y axe are also in symmetry.

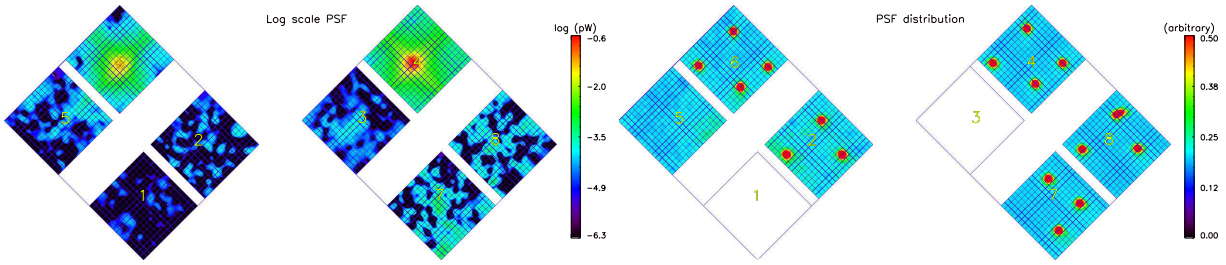

Figure 6. Left: Image of a point source on the PILOT focal plane. The left and right part of the figure show the Transmission and Reflection arrays respectively, as projected on the sky with the elevation axis increasing upward and the cross-elevation axis being horizontal. The intensity is in log scale. Right: Distribution of PSF shapes on the PILOT focal plane for the X,Y,Z=0,0,0 defocus position.

Figure 7 shows the average PSF obtained from a 12×12 microscaning pattern over a region of ± 2 pixels around pixel $(3, 7)$ of array #6. Figure 7 shows the comparison between the above PSF and the modelled PSF. The observed PSF shows reasonably good agreement with the modelled PSF.

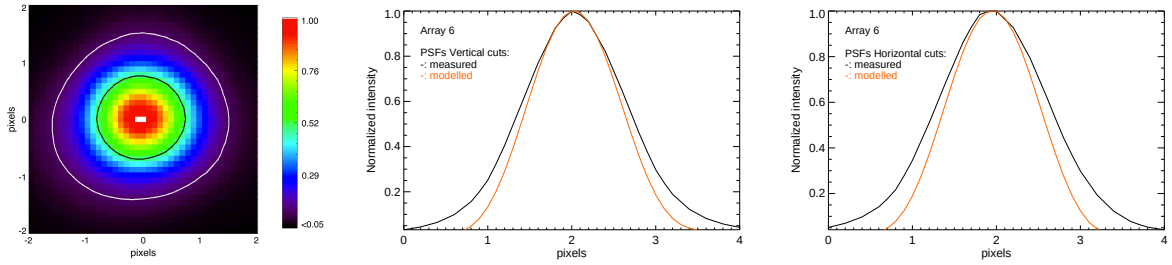

Figure 7. Left: Image of the average PSF obtained from a 12×12 microscaning pattern over a region of ± 2 pixels around pixel $(3, 7)$ of array #6. Contour levels are at 1.0, 0.5 and 0.1. Center and Middle: The vertical (center) and horizontal (middle) normalized cuts across the measured PSF (black) and the modelled PSF (red).

Table 1. Elevation-averaged focal plane geometry parameter values obtained. The vertical line separates arrays from the transmission (TRANS) and reflexion (REFL) array respectively.

Array	δ_x '/pix	δ_y '/pix	α degree	x_0 pix	y_0 pix	δ^0_{cel} pix	δ^0_{el} pix
2	-1.476±0.016	1.480±0.009	-46.481±0.452	7.5±0.0	7.5±0.0	22.405±0.371	-5.255±0.302
6	-1.530±0.006	1.416±0.006	-43.470±0.101	7.5±0.0	7.5±0.0	-4.851±0.379	20.557±1.234
5	-1.488±0.003	1.476±0.002	-42.219±0.174	7.5±0.0	7.5±0.0	-22.777±0.327	2.054±1.162
4	1.529±0.004	1.418±0.010	44.414±0.264	7.5±0.0	7.5±0.0	-4.688±0.345	20.630±1.252
8	1.478±0.001	1.483±0.003	47.369±0.405	7.5±0.0	7.5±0.0	22.147±0.344	-5.965±0.314
7	1.513±0.005	1.498±0.006	46.183±0.260	7.5±0.0	7.5±0.0	3.406±0.435	-24.456±1.312

4.2 FOCAL PLAN GEOMETRY

The aim of this test is to establish the precise correspondance between positions in the focal plane and directions in the sky. For this test, the sub-millimeter bench shown in Fig. 4 was used without polarizer. The collimator was calibrated using a theodolit to provide the correspondence between source displacement at the focus of the collimator (X_S, Y_S) and the elevation and cross-elevation offsets of the source $(\Delta_{el}; \Delta_{cel})$ direction.

We measure the PILOT focal plan geometry using the collimator source positionned at the centre and the 4 corners of each array, at several elevations of the collimator (23, 30, 45 and 49°). Each (X_S, Y_S) position of the source and the associated elevation and cross-elevation angles with respect to the center of the instrument focal plane have been measured, are dated by the on board computer and saved with the data. For each position of the source, we compute the average PSF image from the average ON and OFF images according to the collimator shopper position. Each PSF is fitted using a 2D Gauss fitting procedure.

We fit the following system:

$$\begin{pmatrix} \Delta_{cel} - \delta^0_{cel} \\ \Delta_{el} - \delta^0_{el} \end{pmatrix} = \begin{pmatrix} \delta_x \\ \delta_y \end{pmatrix} \begin{pmatrix} cos(\alpha) & sin(\alpha) \\ -sin(\alpha) & cos(\alpha) \end{pmatrix} \begin{pmatrix} x - x_0 \\ y - y_0 \end{pmatrix} \quad (1)$$

where x and y are the measured pixel position of the peak of the PSFs along the array directions, x_0 and y_0 are the pixel position of the rotation center, α is the rotation angle, and δ_x and δ_y are the pixel scale along the array directions. Δ_{cel} and Δ_{el} are the known cross-elevation and elevation offsets of the collimator source compared to a reference position (API). δ^0_{cel} and δ^0_{el} are the cross-elevation and elevation offset between the API and the reference pixel (x_0,y_0). We let δ_{cel} and δ_{el}, α, δ^0_{cel} and δ^0_{el} be free parameters. x_0, y_0 are set at the center of each array.

The average focal plane geometry parameter values derived for each arrays fitting Eq. 1 are given in Tab. 1. Uncertainties given in the table are computed from the standard deviation of free parameters for the various elevations.

4.3 BACKGROUND AND OFFSETS

The aim of these tests is to measure the amplitude and spatial shape of the background. These measurements are also used to derive the electronic offsets of the detectors and to measure the instrumental polarization. For these tests, the experience has been placed under a controlled Nitrogen atmosphere (relative humidity $< 2\%$) in order to diminish absorption between the emission source and the instrument, which is mostly contributed by water in the atmosphere.

Three configurations were used for these tests: First, a $1m^2$ eccosorb sheet, acting as a room temperature black body, was placed in front of the whole instrument, covering the whole the whole instrument field of view. Second, the PILOT primary mirror was removed and a tank containing eccosorb maintained either at room temperature or at Liquid Nitrogen ($77K$) temperature was inserted in from of the photometer, aginst covering the whole FOV of the instrument.

The measurement m_T and m_R on the Transmission and Reflexion arrays of PILOT are related to the radiation intensity I, polarization fraction p and polarization angle ψ through

$$m_T = \frac{1}{2}R^T_{xy} \times T^T_{xy} I \times (1 + p\cos 2\psi \cos 4\omega + p \sin 2\psi \sin 4\omega) + O^R_{xy}\,; \quad (2)$$

$$m_R = \frac{1}{2}R^T_{xy} \times T^T_{xy} I \times (1 - p\cos 2\psi \cos 4\omega - p \sin 2\psi \sin 4\omega) + O^T_{xy}. \quad (3)$$

where T_{xy} is the optics transmission and R_{xy} is the detector response. ω is the angle between the HWP fast axis and the vertical direction. O^R_{xy} and O^T_{xy} are the electronic offsets for Reflection and Transmission arrays respectively.

For each pixel, we fit the signal as a function of HWP angle using

$$m_T = A^T_0 + A^T_1 \cos 4\omega + A^T_2 \sin 4\omega\,; \quad (4)$$

$$m_R = A^R_0 - A^R_1 \cos 4\omega - A^R_2 \sin 4\omega\,. \quad (5)$$

where the fitted parameters A_0, A_1, A_2 are related to the polarization parameters I, ψ and p as

$$I = 2(A_0 - O_{xy})/\mathcal{R}_{xy} \quad (6)$$

$$p = \frac{1}{2} atan(A_2, A_1)(+\pi/2 for Rarray) \quad (7)$$

$$\psi = \frac{(A_1^2 + A_2^2)^{1/2}}{A_0 - O_{xy}/2}. \quad (8)$$

Assuming that the background sources at 300 K and 77 K have the same flat true spatial distribution and that the intensity is proportional to temperature (the Rayleigh-Jeans approximation for Black-Bodies), ie $I(T) \propto T$,

$$A_0(300K) - A_0(77K) = \frac{1}{2} R_{xy} T_{xy} (300 - 77). \quad (9)$$

The optical transmission (or the shape of the background illumination on the detector) is then given by

$$T_{xy} = \frac{2(A_0^{300K} - A_0^{77K})}{(300 - 77) R_{xy}}. \quad (10)$$

Alternatively, the offsets on both focal planes can be computed using Eq. 6 applied to one of the background measurements and by replacing T_{xy} using Eq. 10, as

$$O_{xy} = A^T_0 - \frac{1}{2} T R_{xy} T_{xy} = \frac{77 A_0^{300K} - 300 A_0^{77K}}{(77 - 300)}. \quad (11)$$

Note that the offsets are independent of the system response $\mathcal{R}_{xy}$.

The obtained background images are shown in Fig. 8. The color scale is such that the dynamics in the two images is the same. At 300 K, the background levels are between 3.5 and 9 pW/pix, and they are correspondingly lower at 77 K. The background images show lower values at the center of the focal plane, and larger values in outer regions. The variations are $\simeq$30 % and 24 % at 300 K and 77 K respectively. This is likely due to vignetting by the optics, in particular by lens L2 which has a large curvature.

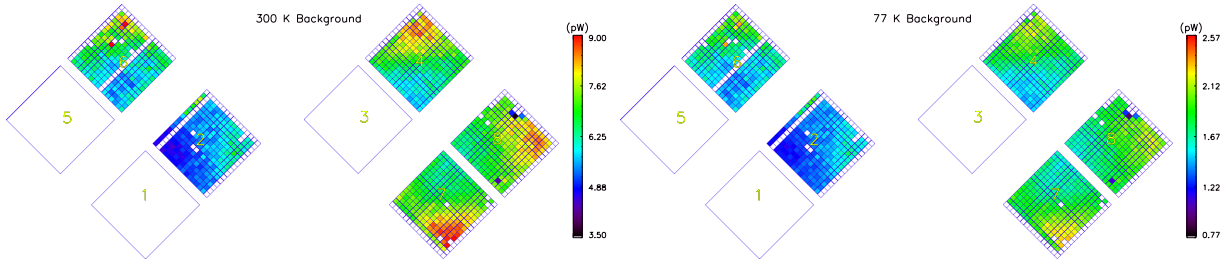

Figure 8. Map of the measured background for the background at 300 K (left) and 77 K (right) in the PILOT focal plane. The color scale is such that the dynamics in the two images is the same.

4.4 POLARIZATION

In order to characterize the polarization performances of the experiment, we use a large format (1×1 m) polarizer, developed originally for the ARCHEOPS experiment, hereafter refered to as ArchPol. The ArchPol polarizer is composed of an array of 3×3 frames hosting a large number of metal wires (50 μm thickness, 100 μm separation) and was initially optimized for millimeter wavelengths. The polarizer is inserted in the beam of the collimator as shown in Fig. 4, and can be rotated, in order to produce a polarized source with any polarization direction. Assuming that polarization cross talk of the PILOT instrument is negligible, the polarizer was shown to provide a source polarization fraction higher than 73% in the PILOT 240 μm band. The wire direction of each frame constituting the polarizer was measured with theodolites and laser-tracker. The median wire direction was measured with respect to the polariser mechanical structure with a accuracy of about $2.4'$. A series of optical reference balls associated with the polarizer structure allow us to measure its orientation with an accuracy of $1.4''$. Globally, the direction of linear polarization is known to an accuracy of about $2.4'$, with respect to the instrument.

Assuming that the polarization splitting grid inside the has PILOT photometer has negligible cross-polarization, it can be shown that the total power measured by the detectors of the transmission and reflection arrays can be expressed as

$$\begin{aligned} m_T &= 1 + \frac{1+2\gamma}{2} k \cos 2\alpha + (k\beta \cos 2\alpha + \beta) \cos 2\omega + k\beta \sin 2\alpha \sin 2\omega \\ &+ \frac{1-2\gamma}{2} k \cos 2\alpha \cos 4\omega + \frac{1-2\gamma}{2} k \sin 2\alpha \sin 4\omega \end{aligned} \quad (12)$$

$$\begin{aligned} m_R &= 1 - \frac{1+2\gamma}{2} k \cos 2\alpha + (k\beta \cos 2\alpha - \beta) \cos 2\omega + k\beta \sin 2\alpha \sin 2\omega \\ &- \frac{1-2\gamma}{2} k \cos 2\alpha \cos 4\omega - \frac{1-2\gamma}{2} k \sin 2\alpha \sin 4\omega \end{aligned} \quad (13)$$

where β is the differential transmission between the fast and slow axis of the HWP, γ is the phase shift induced by the HWP thickness. α is the polarization angle of the incident radiation given by the angular position of ArchPol. k is the cross-polarization of the ArchPolpolarizer. For a perfect HWP, $\beta = 0$ and $\gamma = -0.5$ and Eq. 12 and Eq. 13 have no term in 2ω.

4.4.1 ArchPol CHARACTERIZATION

Another reasonable assumption is that the HWP is very good (which will be checked in the next section) or at least that its imperfections are small compared to the likely poor cross-polarization expected from large diameter ArchPol, designed to work at wavelengths larger than 850μ. We therefore assume in this section that $\beta = 0$ and $\gamma = -0.5$. Equations (12) and (13) therefore reduce to:

$$m_T = 1 + k \cos 2\alpha \cos 4\omega + k \sin 2\alpha \sin 4\omega \quad (14)$$

$$m_R = 1 - k \cos 2\alpha \cos 4\omega - k \sin 2\alpha \sin 4\omega \quad (15)$$

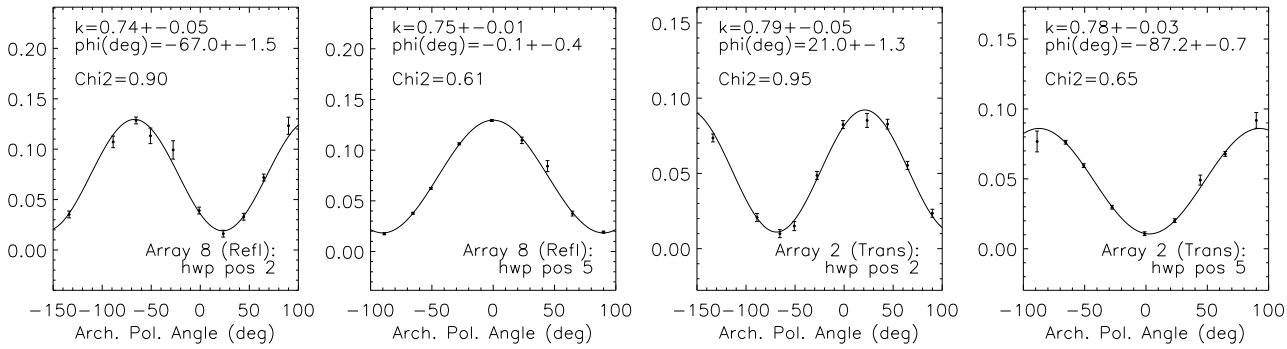

Figure 9. Peak flux of the PSF fitted on arrays 2 and 8 for positions 2 (-40.25^o) and 5 (-2.75^o) of the HWP, as a function of the nine angular positions of ArchPol. Error bars have been derived a posteriori.

These observations for two positions of the HWP and nine positions of ArchPol are presented on Fig. 9. The best fit shown in the figure are consistent with a polarization fraction of ArchPol between $k = 0.75\%$ and $k = 0.79\%$. Measures of ArchPol's cross-polarization k are consistent for each HWP position on a given array but marginally consistent between the two arrays when the HWP is in position 5 and uncertainties on k are best.

4.4.2 HALF WAVE PLATE CHARACTERIZATION

We take the values of k derived for the transmission and the reflection arrays in section 4.4.1 and now fit the peak of the PSF as a function of the HWP angle for a fixed orientation of ArchPol(Figs.10 and 11). If the HWP is good, β should be close to zero, there should be no term in 2ω in the fit should be good with terms in 4ω only. This can be seen on the solid line fits. Allowing for terms in 2ω (dash line) leads to inconsistent determinations of β with no significant improvements of the goodness of fit (although error bars are still determined a posteriori here). This, together with the finding that $\gamma = -0.5 \pm 0.04$ using the transmission array and $\gamma = -0.49 \pm 0.02$ using the reflection array indicates that the HWP is indeed performing as well as expected.

We fit the observed source fluxes independently for the Reflection and Transmission arrays, using

$$m_T = a_0 + a_1 \cos 4\omega + a_2 \sin 4\omega, \tag{16}$$

where a_0, a_1 and a_2 are free parameters, related to physical parameters through

$$\alpha = \frac{1}{2} \arctan \frac{a_2}{a_1} \tag{17}$$

$$\rho_{T,R} = \frac{\max(m_{T,R}) - \min(m_{T,R})}{\max(m_{T,R}) + \min(m_{T,R})} = \frac{a_0}{\sqrt{a_1^2 + a_2^2}} \tag{18}$$

$$\gamma_T = \frac{2 - k\rho_T + k\cos 2\alpha}{-2k\rho_T - 2k\cos 2\alpha} \tag{19}$$

$$\gamma_R = \frac{2 - k\rho_R - k\cos 2\alpha}{-2k\rho_R + 2k\cos 2\alpha} \tag{20}$$

The best fit are shown in Fig. 10 and Fig. 11.

No evidence has been found for a significant differential transmission between the fast and slow axis of the HWP ($\beta = 0$) and no evidence has been found either for a defect related to the phase shift ($\gamma = -0.5 \pm 0.04$ or -0.49 ± 0.02).

4.4.3 POLARIZATION ROTATION

Optical calculations show that the direction of an incident linear polarization can be slightly rotated through the optics, as it propagates from the primary mirror to the detector. This rotation angle varies across the

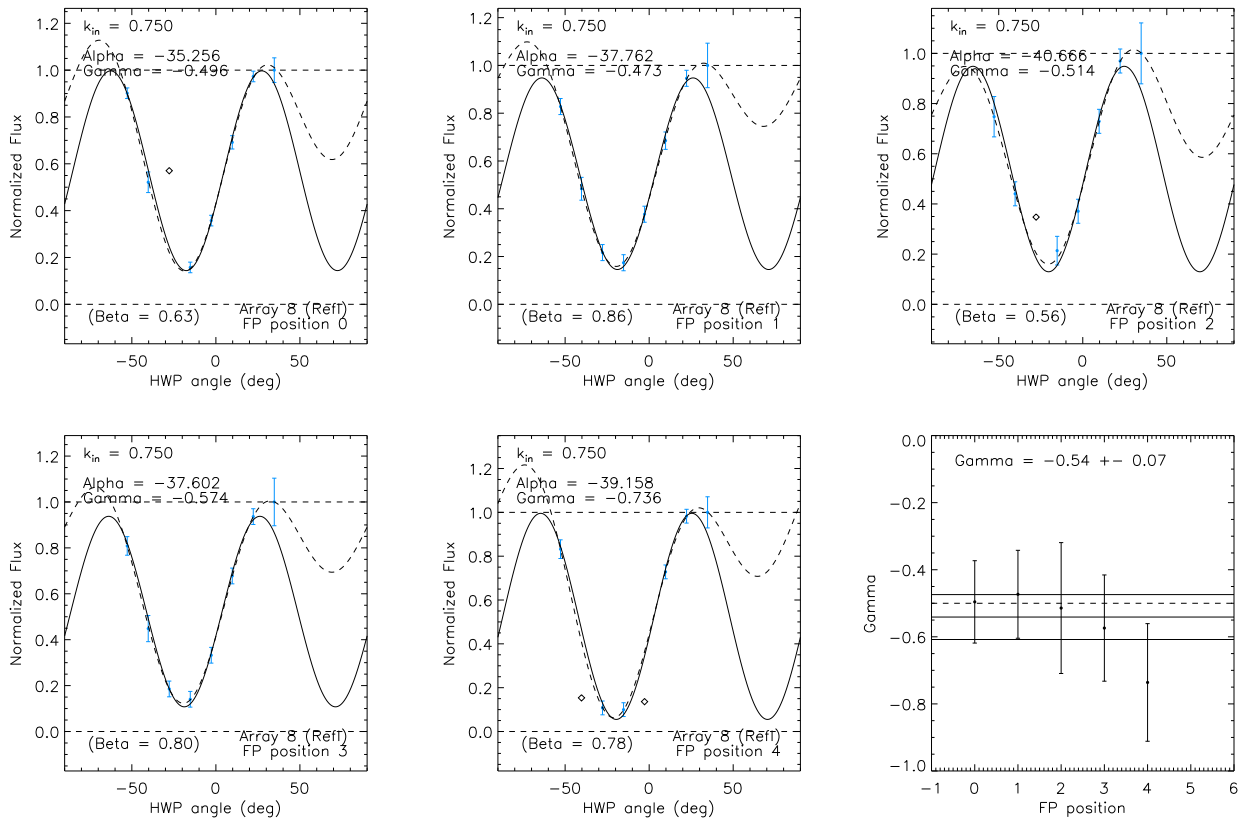

Figure 10. Peak flux of the PSF fitted on array 8 for 5 positions on the array as a function of the HWP angle. Error bars have been derived a posteriori. Data points marked as black empty diamonds have been discarded for the fit. On the last plot, the dash line indicates the theoretical perfect value $\gamma = -0.5$, the solid lines are the average value for γ and its one σ uncertainty.

focal-plane, and, according to calculations, can reach a few degrees away from the optical axis. This rotation must be measured precisely and taken into account during astronomical data processing. To characterize this rotation, the whole focal plane has been scanned with the polarizer set at different polarization directions, in order to measure the polarization distortion. For each position, the direction of the polarizer has been measured as described above.

We used the polarizer at angles $45.19 \pm 0.30^{\circ}$ deg and $-44.81 \pm 0.30^{\circ}$ and moved the polarized collimator point source over 25 pixels of each array. At each position, we rotated the HWP over its full angle range (8 positions). The data is averaged for each PSF position and the PSF flux as a function of HWP position is fitted using Eq. 16 in order to derive polarization parameters. Figure 12 shows the distribution of polarization angles over the focal plane. It can be seen that the polarization direction is recovered with the right angle. The actual average recovered values are 45.39° and -42.6°. We evidence a systematic rotation across the focal plane with an amplitude of about 3° (see Fig. 13).

5. CONCLUSIONS

We have performed a series of ground test of the PILOT experiment, using a collimated source and a large diameter polarizer. We used this system to control the optical performances of the instrument. We measured the width of the PSF of the instrument as a function of defocusing of the primary mirror and found the optimum defocus. The analysis of the PSF shape shows that the optical system conforms to expectations. We also used the tests to reconstruct accurately measure the geometry of the focal plane. Results in polarization indicate

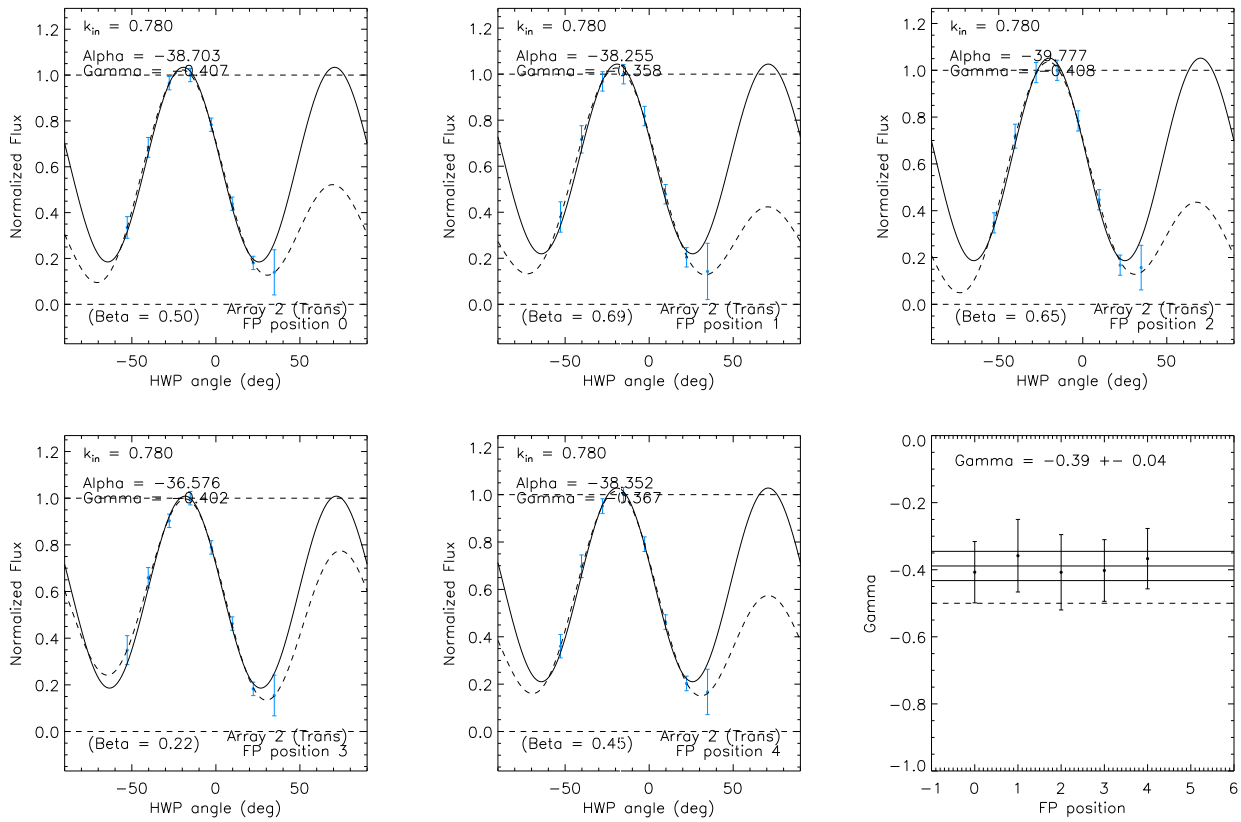

Figure 11. Peak flux of the PSF fitted on array 2 for 5 positions on the array as a function of the HWP angle. Error bars have been derived a posteriori. Data points marked as black empty diamonds have been discarded for the fit. On the last plot, the dash line indicates the theoretical perfect value $\gamma = -0.5$, the solid lines are the average value for γ and its one σ uncertainty.

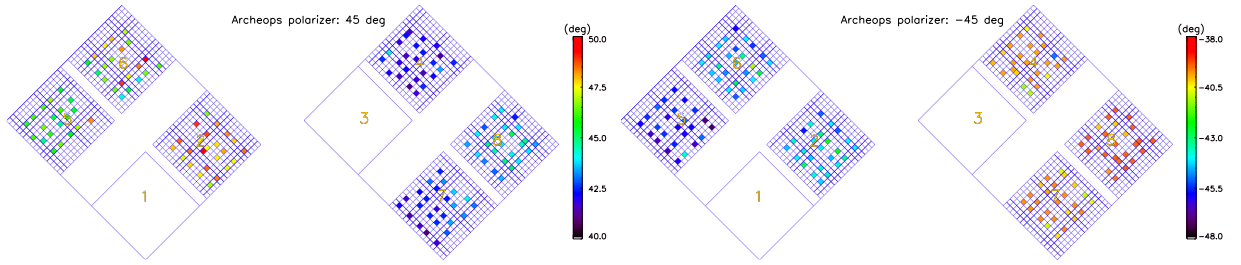

Figure 12. Map of the recovered polarization angles for point sources placed at various locations in the PILOT focal plane. The input linear polarization direction was 45.19 ± 0.30^{o} (left) and -44.81 ± 0.30^{o} (right).

that the large scale polarizer used has a 73 % polarization efficiency at 240 μm. We tested the performances of the Half-Wave plate internal to the PILOT photometer and found no evidence for deviation from perfection. We measured the focal plane distribution of polarization directions for a given direction of the point source polarization and evidenced small rotation by the optical system. We used background measurements at various temperatures to separate optical vignetting and electronics or detector offsets. These tests demonstrated that the optics of the PILOT system meets requirements. The data obtained during those tests will be critical to analyze the first scientific data, that will be obtained during the first stratospheric balloon flight of the instrument, in 2015.

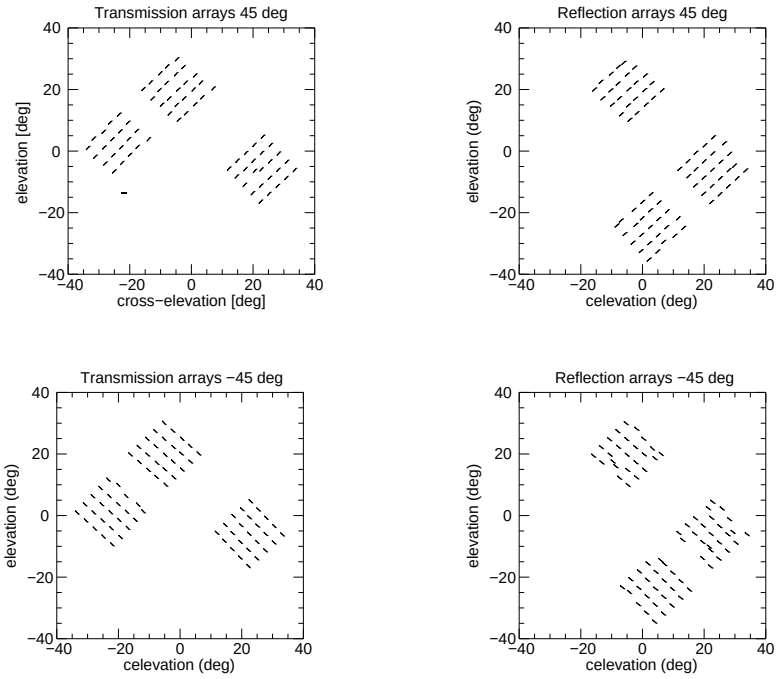

Figure 13. Map of the recovered polarization angles for point sources placed at various locations in the PILOT focal plane. The input linear polarization direction was $45.19 \pm 0.30^{\circ}$ (left) and $-44.81 \pm 0.30^{\circ}$ (right).

REFERENCES

1. Page, L., Hinshaw, G., Komatsu, E., Nolta, M. R., Spergel, D. N., Bennett, C. L., Barnes, C., Bean, R., Doré, O., Dunkley, J., Halpern, M., Hill, R. S., Jarosik, N., Kogut, A., Limon, M., Meyer, S. S., Odegard, N., Peiris, H. V., Tucker, G. S., Verde, L., Weiland, J. L., Wollack, E., and Wright, E. L., "Three-Year Wilkinson Microwave Anisotropy Probe (WMAP) Observations: Polarization Analysis," *ApJS* **170**, 335–376 (June 2007).
2. Fosalba, P., Doré, O., and Bouchet, F. R., "Elliptical beams in CMB temperature and polarization anisotropy experiments: An analytic approach," *PhRvD* **65**, 063003 (Mar. 2002).
3. Hildebrand, R. H., Dotson, J. L., Dowell, C. D., Schleuning, D. A., and Vaillancourt, J. E., "The Far-Infrared Polarization Spectrum: First Results and Analysis," *ApJ* **516**, 834–842 (May 1999).
4. Benoît, A. and Archeops Collaboration, "ARCHEOPS: a balloon experiment for measuring the cosmic microwave background anisotropies," *Advances in Space Research* **33**, 1790–1792 (Jan. 2004).
5. Benoît, A., Ade, P., Amblard, A., Ansari, R., Aubourg, É., and et al., "First detection of polarization of the submillimetre diffuse galactic dust emission by Archeops," *A&A* **424**, 571–582 (Sept. 2004).
6. Planck Collaboration Int. XXI, "Planck intermediate results. XXI. Comparison of polarized thermal emission from Galactic dust at 353 GHz with optical interstellar polarization," *A&A, submitted, [arXiv:astro-ph/1405.0873]* (2014).
7. Planck Collaboration Int. XIX, "Planck intermediate results. XIX. An overview of the polarized thermal emission from Galactic dust," *A&A, submitted, [arXiv:astro-ph/1405.0871]* (2014).
8. Planck Collaboration Int. XX, "Planck intermediate results. XX. Comparison of polarized thermal emission from Galactic dust with simulations of MHD turbulence," *A&A, submitted, [arXiv:astro-ph/1405.0872]* (2014).
9. Hildebrand, R. H., Kirby, L., Dotson, J. L., Houde, M., and Vaillancourt, J. E., "Dispersion of Magnetic Fields in Molecular Clouds. I," *ApJ* **696**, 567–573 (May 2009).

10. Finkbeiner, D. P., Davis, M., and Schlegel, D. J., "Extrapolation of Galactic Dust Emission at 100 Microns to Cosmic Microwave Background Radiation Frequencies Using FIRAS," *ApJ* **524**, 867–886 (Oct. 1999).
11. Meny, C., Gromov, V., Boudet, N., Bernard, J., Paradis, D., and Nayral, C., "Far-infrared to millimeter astrophysical dust emission. I. A model based on physical properties of amorphous solids," *A&A* **468**, 171–188 (June 2007).
12. Planck Collaboration I, "*Planck* 2013 results: Overview of Planck Products and Scientific Results," *A&A, in press* (2014).
13. Planck Collaboration Int. XVII, "Planck intermediate results. XVII. Emission of dust in the diffuse interstellar medium from the far-infrared to microwave frequencies," *A&A, in press* (2014).
14. Planck Collaboration XI, "*Planck* 2013 results: All-sky model of thermal dust emission," *A&A, in press* (2014).
15. Molinari, S., Swinyard, B., Bally, J., Barlow, M., Bernard, J.-P., Martin, P., Moore, T., Noriega-Crespo, A., Plume, R., Testi, L., Zavagno, A., and et al., "Hi-GAL: The Herschel Infrared Galactic Plane Survey," *PASP* **122**, 314–325 (Mar. 2010).
16. Engel, C., Ristorcelli, I., Bernard, J.-P., Longval, Y., Marty, C., Mot, B., Otrio, G., and Roudil, G., "Characterization and performances of the primary mirror of the PILOT balloon-borne experiment," *Experimental Astronomy* **36**, 21–57 (Aug. 2013).